Available online at www.sciencedirect.com

ScienceDirect

IFAC Papers Online CONFERENCE PAPER ARCHIVE

IFAC PapersOnLine 54-20 (2021) 475–481

A High-Fidelity Modeling Framework for Near-Field Electrohydrodynamic Jet Printing

Nazanin Farjam * **Isaac A. Spiegel** * **Kira Barton** *

* *Department of Mechanical Engineering, University of Michigan, Ann Arbor, MI 48109, USA*

Abstract: Electrohydrodynamic jet (e-jet) printing is a high-resolution, jet-based micro-additive manufacturing process that has gained momentum in many applications such as printed electronics. However, there are limited works in the literature that have modeled the e-jet process due to its multi-physics and multi-phase nature. This work presents a high-fidelity, two-phase framework for the high-resolution e-jet printing process based on the leaky-dielectric model and two-phase flow (liquid-air). The level set method is used to track the ink-air interface, as a suitable choice for high-resolution two-phase processes. We have developed the model in COMSOL Multiphysics, where we relaxed some of the prior art's assumptions, including that of a constant flow rate to the nozzle inlet, which is typically not accurate for the e-jet process at high-resolution. The simulation is conducted for a conventional near-field e-jet setup and the results successfully demonstrate the critical process steps including equilibrium, Taylor Cone formation, and the creation of a jet. Moreover, to evaluate the model, the effects of different material properties such as surface tension, viscosity, and relative permittivity on the e-jet process are simulated and discussed.

Keywords: high-fidelity model, additive manufacturing, e-jet printing, leaky-dielectric

1. INTRODUCTION

Despite the ever increasing demand for additive manufacturing (AM) technology, there are gaps in high-fidelity process modeling and material prediction that lead to slow and costly process optimization through experimental testing. Most AM processes, such as selective laser melting (SLM) or jet-based printing, are associated with sophisticated multi-physics. Therefore, when it comes to their control design, developing high-fidelity models offers advantages, such as: (i) allowing for a better understanding of complicated physical AM systems that will lead to more informed model reductions and assumptions that can be made when transitioning to simplified modeling approaches for control design, (ii) providing a platform for obtaining optimized working parameters for desired jet behavior depending on the material interactions and device application, and (iii) developing a simulation environment for evaluating simplified AM models for control design.

Electrohydrodynamic jet (e-jet) printing is a novel high-resolution (50nm - 50um) micro additive manufacturing (μ-AM) technique with the ability to print a wide range of materials including biomaterials, conductive nanoparticle suspensions and viscous polymers, Onses et al. (2015); Park et al. (2007), resulting in many novel applications, Farjam et al. (2020); Cho et al. (2020). This technology uses an electric potential between a conductive microscale nozzle filled with an ink material and a substrate to issue a jet of ink material from the nozzle towards the substrate. An e-jet-printed pattern is the result of droplet ejection, droplet spread on the substrate, and its coalescence behavior, Pannier et al. (2017). Current modeling works in the literature can be divided into two categories: methods that focus on the jetting dynamics, Wright et al. (1993); Yang et al. (2014); Spiegel et al. (2017, 2020), and those that describe the spreading and coalescence behavior of the droplets on the substrate, Pannier et al. (2017, 2019). The focus of the work presented in this paper is on the jetting dynamics.

There are several factors that limit the applicability of the above-mentioned frameworks in this category. Some of these models are physics-based frameworks, Wright et al. (1993); Yang et al. (2014), that leverage simplified first principle physics to describe the e-jet printing process. Importantly, these frameworks are limited to the meniscus evolution before jetting. They are unable to capture precise jetting dynamics, because the jet formation at the meniscus makes the capacitor geometry and fluid flow more complicated than what can be described using the simplified first principles. Other studies have leveraged both data-driven and physics-based models for a proposed hybrid modeling framework for high-resolution e-jet printing, Spiegel et al. (2017, 2020). Although these frameworks are well-suited for control algorithms, their data-driven components require more time and resources for collecting data since they are neither scalable to different nozzle sizes or offsets from the substrate, nor flexible to different ink materials. Moreover, it may be prohibitively challenging to collect data of adequate quality at high resolutions due to physical limitations of the microscopy techniques used.

⋆ This work was supported by the National Science Foundation grant CMMI-1727918.

10.1016/j.ifacol.2021.11.218

Therefore, there is a need for a high-fidelity physics-based model that can account for various material properties and e-jet process parameters, and provide a more realistic estimation of the jetting dynamics that are observed in experimental testing.

The presented work offers the following benefits over existing models that describe the high-resolution e-jet process in the literature:

- Flexibility to system parameters such as a wide range of material properties, voltage signal values and setup geometry.
- Ability to capture high-resolution jet formation, which helps with an understanding of the physics that drives printing performance.

The rest of the paper is structured as follows. First, a thorough background is provided for the e-jet process and the state-of-the-art. Section III provides the model description including the governing physics that are coupled to explain the e-jet dynamics, and the model setup including the geometry, boundary conditions and the initial values. In section IV, results for a conventional high-resolution e-jet setup and the effect of different material properties on the process are provided. The last section provides a conclusive summary of the work and areas for future research.

2. BACKGROUND

2.1 Electrohydrodynamic jet printing

E-jet printing is a phenomenon that is governed by electrohydrodynamics. As depicted in Fig. 1a, the conventional E-jet printing setup includes a conductive micro-capillary nozzle filled with an ink material and a substrate, where the voltage is applied to the nozzle and the substrate is grounded. The electric potential between the nozzle and the substrate leads to the substrate acting as an extractor for the ink material at the nozzle tip. The important geometric parameters of the printing setup include nozzle radius, standoff height, and nozzle length. Figure 1b depicts high-speed images of jetting dynamics under a DC or a pulse voltage signal.

At low voltage (V_l) the meniscus may rest at stable equilibrium, with the electrostatic force balanced against opposing forces such as viscous force and the force due to surface tension. At equilibrium the meniscus shape is often approximately a spherical cap. When a DC high voltage is applied to the nozzle, electric charge accumulates at the meniscus, and creates an electric force in the downward direction resulting in the deformation of the meniscus from a spherical cap shape to a conical shape called a "Taylor Cone". When the voltage is high enough, the electric force overcomes the opposing forces such as surface tension force and viscous force, and a continuous jet is generated from the nozzle tip toward the substrate. This jet continues until a critical amount of charge deposits on the substrate, and the induced electric force becomes weak enough that the ink surface tension dominates and it breaks the jet from the middle resulting in a deposited droplet on the substrate. The surface tension then retracts the ink back to the nozzle tip. During DC printing, the jetting process is defined by the natural dynamics of the ink material; i.e. the

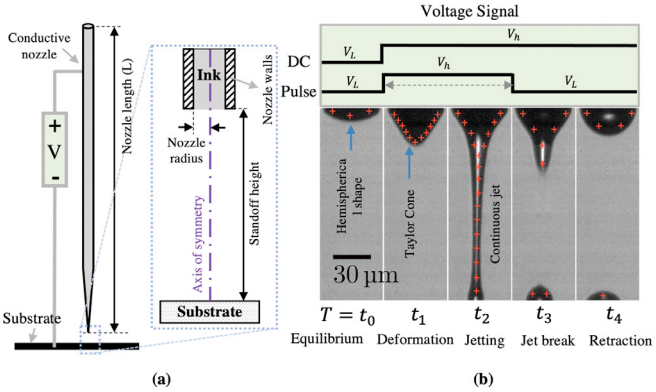

Fig. 1. **Graphical Description of E-jet Printing.** (a) E-jet printing setup identifying the geometrical parameters, and (b) high speed images of jetting dynamics under a DC or pulse voltage signal over time, T. V is the applied voltage signal, and V_l, V_h, and T_p are low voltage, high voltage and pulse width, respectively.

electrohydrodynamics generated by the applied voltage. During this mode, the user does not control the on/off switch of the jetting, but relies on the dynamics of the ink.

An alternative method is called drop-on-demand, where a pulsed voltage is applied to the nozzle. In pulse printing, when the voltage is stepped high (V_h, generally higher than in the DC printing mode), similar to DC printing, the increasing electric charge at the meniscus deforms the shape to a Taylor Cone, and eventually results in a fine continuous jet focused toward the substrate. When the pulse width (T_p) is smaller than the time at which the jet would break naturally, we are in the subcritical regime. In this mode, the user controls the process by defining the pulse width, i.e. the on/off switch for the jetting process. In this work, we have focused on the jetting initiation, which is defined by the same physics for both DC and pulse printing.

2.2 State-of-the-art

While the multiphase, multiphysics nature of e-jet printing has led to a higher tendency toward experimental research, there have been some notable works on modeling and simulation.

A "leaky-dielectric" model that explains the electrohydrodynamic behavior of droplets was introduced by Melcher and Taylor (1969), and the model was later elaborated by Saville (1997). Under the category of electrohydrodynamics, most of the related modeling works in the literature have concentrated on electrohydrodynamic atomization and electrowetting, e.g. Lastow and Balachandranb (2006); Roghair et al. (2015). Some researchers have leveraged numerical methods to simulate and analyze e-jet phenomenon using commercial software. Pan and Zeng (2019) proposed a numerical simulation model of the droplet generation process for e-jet using FLOW-3D software, and validated the model experimentally. Mohammadi et al. (2019) simulated the e-jet process under a pulse voltage in COMSOL, and Zhao et al. (2019) simulated a coaxial e-jet process using the same software. The foundation of

the solvers used by the mentioned studies was the leaky-dielectric model. While all of these simulation models provide benefits for some applications, they have been studied at scales significantly larger than typical high-resolution e-jet printing, which is defined by near-field interactions (standoff heights below 300 μm nozzle sizes less than 50 μm resulting in the generation of a 10 μm or less jet diameter). A recent paper by Singh and Subramanian (2020) simulated a high resolution e-jet printing process; however, similar to the other existing frameworks, they only considered a constant flow rate at the nozzle inlet, while in reality, flow rate changes for different voltage signals, Spiegel et al. (2020). Importantly, in high-resolution e-jet printing, the assumption of a constant flow rate or external force at the nozzle inlet is not accurate. Therefore, the applicability of these solvers for accurately representing high-resolution e-jet is unknown. In this work, we develop a high-fidelity modeling framework in COMSOL Multiphysics that addresses the limitations of the existing methods to capture high-resolution electrohydrodynamic jet formation for a step voltage input.

3. MODEL DESCRIPTION

The e-jet phenomenon involves multiphysics that govern the system behavior making the modeling problem more challenging. In the first part of this section, we describe the different classes of physics that govern the e-jet process. In the second part, the equations used to describe these physical behaviors as well as the coupling between them are provided. In this work, e-jet physics is described based on the leaky-dielectric model, Saville (1997), similar to the related works in the literature, with the addition of the following contributions:

- Relaxing the assumption of a constant flow rate at the nozzle inlet.
- Incorporating capillary force to the ink material boundary along its interface with the nozzle.

3.1 Governing physics

The physics that govern the e-jet printing process are demonstrated in Fig. 2. Three core behaviors based on fluid flow, electric field interactions, and interface dynamics between two-phase materials have been identified. Additionally, applied forces to the fluid are illustrated as external forces that influence the jetting dynamics.

The general fluid motion during the e-jet printing process is governed by Newton's second law of motion, i.e. the Navier-Stokes equation for viscous fluids. An external input to Navier-Stokes is the gravity force (F_g) applied in the direction of jetting. The electric field distribution between the nozzle and the substrate is governed by electrostatics, i.e. Gauss's law. The electric field generates an external force (F_E) to the ink material, which is responsible for the Taylor cone formation and jetting of the ink material. The two-phase nature of the e-jet process (ink and air) requires tracking of the ink-air interface, which is governed by two-phase flow physics.

The interface tracking physics can be used to calculate two external forces that are applied to the ink material: surface tension and capillary forces. A surface tension force (F_γ) is applied at the ink-air interface and runs perpendicular to the surface in an inward direction. The directionality stems from cohesive forces that are present in all liquid ink molecules and result in a net zero force on any internal ink molecule. However, surface molecules are only pulled from one side, the interface with other ink molecules, resulting in an inward force defined as a surface tension force that opposes the jetting process. The capillary force directs ink material travel through the nozzle body and to the nozzle tip. Capillary pressure occurs due to the interactions between two immiscible fluids and solid walls of a thin tube, where the resulting force can either oppose or contribute to the fluid travel along the tube depending on the interactions of the two fluids on the solid material. For instance, in the case of e-jet, if the ink material has good wettability on the walls of a glass capillary, meaning that the contact angle of the ink material inside the glass capillary (i.e. θ in Fig. 2) is less than 90 degrees, it indicates that the ink wets the glass nozzle body, which creates a driving force at the nozzle walls contributing to ink transport toward the nozzle tip. This case is depicted in Fig. 2 on the top figure of the capillary force. On the other hand, if the ink material does not wet the glass capillary walls, it attaches to itself rather than the wall by making a contact angle, θ, greater than 90 degrees (bottom figure of capillary force in Fig. 2) that results in an opposing force to the fluid flow toward the substrate.

3.2 Governing equations

Fluid Flow: Navier-Stokes equations, i.e. the general Newton's second law for fluids, governs the fluid motion and solves for the flow velocity and pressure from momentum conservation and continuity:

$$\underbrace{\rho\frac{\partial u}{\partial t}+\rho(u\cdot\nabla)u}_{\text{inertial term}}= \underbrace{-\nabla p}_{\text{pressure force}}+\underbrace{\nabla\cdot[\mu(\nabla u+(\nabla u)^T)]}_{\text{viscosity force}}+\underbrace{F_{ext}}_{\text{external forces}} \tag{1}$$

$$\nabla\cdot u=0 \tag{2}$$

where ρ, p, μ, and u indicate the fluid density, pressure, fluid viscosity, and fluid velocity, respectively. ∇ denotes the gradient and $\nabla\cdot$ is the divergence operator. The left-hand side of eq. (1) denote the inertial term, i.e. $\rho\frac{Du}{Dt}$, where $\frac{D}{Dt}$ is the material derivative and defined as $\frac{\partial}{\partial t}+u\cdot\nabla$; therefore, $\rho\frac{Du}{Dt}=\rho\frac{\partial u}{\partial t}+\rho(u\cdot\nabla)u$. The first term on the right-hand side is the pressure force, the second term is the viscosity force and F_{ext} denotes the external forces:

$$F_{ext}=F_g+F_E+F_\gamma+F_{wall} \tag{3}$$

where F_g=ρg is the gravity force, and g is the gravity vector. Electric force (F_E), surface tension force (F_γ), and capillary force (F_{wall}) will be expanded later.

Electric Field: Gauss's law calculates the electric field distribution:

$$\nabla\cdot(\varepsilon\nabla V)=\rho_f \tag{4}$$

where ε, V and ρ_f indicate the relative permittivity, electric potential, and charge density, respectively. The

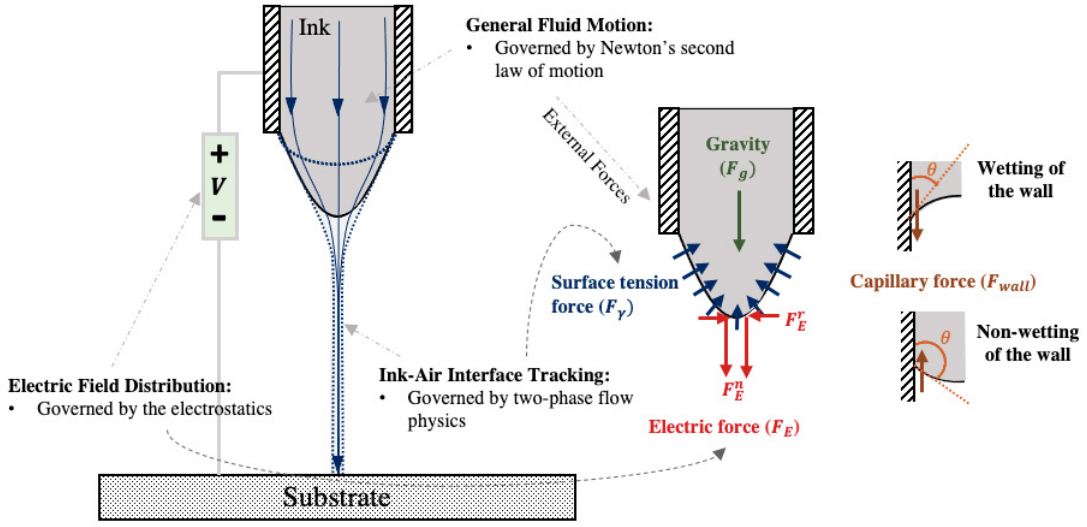

Fig. 2. **Graphical Description of the Governing Physics During the E-jet Printing Process.** The external forces that are applied to the meniscus include gravity force, F_g, electric force, F_E, surface tension force, F_γ, and capillary force, F_{wall}.

relationship between electric field and electric potential is as follows:

$$E = -\nabla V \tag{5}$$

The electric force, F_E, can be calculated by taking the divergence of the Maxwell stress tensor, T:

$$F_E = \nabla \cdot T = \rho_f E - \frac{1}{2}E^2 \nabla \varepsilon \tag{6}$$

The first term is known as the Coulombic force, which acts along the ink-air interface due to the interactions between the electric field and the charged interface. The second term is the force due to the change in the material permittivity along the ink-air interface.

Two-Phase Interface: Tracking the interface is important for modeling the e-jet process due to its two-phase nature. Moreover, the fluid flow and electric field equations described above can be leveraged for solving the physics in each phase of air or ink considering constant material properties throughout a phase including fluid density, viscosity and relative permittivity. However, along the ink-air interface, there will be a smooth transition between the air and ink phase, which leads to a transition in material properties. Therefore, tracking the ink-air interface is required to calculate the volume fraction of each fluid at the interface elements and update material properties at the interface throughout the process.

There are different methods for tracking behavior at the interface between different fluid phases, such as volume-of-fluid (VOF), Pan and Zeng (2019), phase field method, Zhao et al. (2019); Singh and Subramanian (2020), and the level set method (LSM), Mohammadi et al. (2019). In this study, we use the LSM, which is known as a robust and accurate method for high-resolution surface curvature applications due to the smooth transition function of LSM that comes at a cost of high computation time. Non-conservative LSM solves the following equation to move the ink-air interface with the velocity field, u:

$$\frac{\partial \phi}{\partial t} + u \cdot \nabla \phi = \lambda \nabla \cdot (\epsilon_{ls} \nabla \phi - \phi(1-\phi)\frac{\nabla \phi}{|\nabla \phi|}) \tag{7}$$

where ϕ is the level set function and its value ranges from 0 to 1 as the phase transitions smoothly from ink to air. ϵ_{ls} determines the thickness of the region where ϕ goes smoothly from 0 to 1, and λ determines the amount of reinitialization or stabilization of the level set function, which needs to be tuned for each problem. It should be noted that very small values for λ result in numerical instabilities and very large values for λ can lead to unrealistic interface movement. A reasonable estimation for λ is the maximum expected velocity. LSM is coupled with Laminar flow and electrostatics across the ink/air interface through the following equations:

$$\mu = \mu_{ink} + (\mu_{air} - \mu_{ink})\phi \tag{8}$$
$$\rho = \rho_{ink} + (\rho_{air} - \rho_{ink})\phi \tag{9}$$
$$\varepsilon = \varepsilon_{ink} + (\varepsilon_{air} - \varepsilon_{ink})\phi \tag{10}$$

For LSM, the surface tension force acting on the interface between two fluids, F_γ, is then obtained as follows:

$$F_\gamma = \gamma \delta \kappa n + \delta \nabla_s \gamma \tag{11}$$

where n, γ and $\kappa = -\nabla \cdot n$ are the unit normal to the interface, surface tension coefficient, and curvature. δ is a Dirac delta function that is nonzero only at the fluid interface, and is approximated by a smooth function, i.e. $\delta = 6|\nabla\phi||\phi(1-\phi)|$. ∇_s is the surface gradient operator ($\nabla_s = (I - nn^T)\nabla$). The capillary force is applied to the ink material as an external force near the nozzle wall to enforce the contact angle when the ink is traveling inside the nozzle:

$$F_{wall} = \delta\gamma(n_{wall} \cdot n - \cos\theta)n - \frac{\mu}{\beta}u \tag{12}$$

The first term introduces the boundary force to enforce the contact angle, where θ is the contact angle that the fluid material (here, the ink material) makes in contact with the capillary inside wall, n_{wall} is the wall normal, and '·'

denotes dot product. The second term is a frictional force, where β is the slip length.

3.3 Model setup

The model is implemented in COMSOL Multiphysics. Assumptions for the model include:

- Axisymmetric jet formation: With this assumption, based on the experimental observations, the geometry is created in the 2D-axisymmetric domain as demonstrated in Fig. 3. The symmetry axis is shown in the figure, where the system is defined in cylindrical coordinates. Compared to solving the physics in 3D, the 2D-axisymmetric assumption reduces the computational complexity and cost significantly.
- Incompressible and laminar flow: With this assumption, the "laminar flow" module in COMSOL is used to capture the fluid flow, which uses a simplified form of the Navier-Stokes equation, i.e. eq. (1) and reduces the complexity of the problem.
- Non-conductive ink material: With this assumption, the "electrostatics" module in COMSOL is used to solve for the electric field. In the case of conductive materials, an "electric current" module can be used to couple Ohm's law to equations (4) and (5). Since most of the polymer and solvent ink materials that we use in e-jet have a low conductivity, we have added this assumption to reduce the computational time.

The geometry is defined as depicted in Fig. 3 based on the setup dimensions. Some material properties must be identified or measured experimentally including viscosity, μ, density, ρ, permittivity, ε, surface tension, γ and contact angle on the capillary wall, θ.

It is important to define boundary conditions precisely when dealing with computational fluid dynamics problems. Boundary conditions include the set of conditions that are known and necessary constraints for the solution to be satisfied. The boundary conditions for fluid flow and electric field physics are defined in Fig. 3. As mentioned earlier, the related works in the literature have considered a constant flow rate to the nozzle inlet as a boundary condition; however, this is an inaccurate assumption, because it has been shown that the flow rate is a function of applied voltage, Spiegel et al. (2020). Therefore, for the nozzle inlet boundary, we have defined a constant pressure, which is the hydrostatic pressure, $P_0 = \rho g L$, where L is the fluid length (nozzle length in this case). In order to address the capillary force, the boundary condition for the nozzle wall is defined using a "wetted wall" condition under the "multiphysics" module. For the electric field distribution, an electric potential boundary condition is considered at the nozzle wall. We define this electric potential as a voltage signal, i.e. a step function from low voltage, V_l to high voltage V_h. The substrate boundary condition is set as ground ($V = 0$). Furthermore, initial values define the initial behavior of the jetting. These values are also defined in Fig. 3.

An important contribution of this work stems from considering the capillary pressure that is responsible for the ink material traveling through the nozzle body and to the nozzle tip. According to the definition, capillary pressure

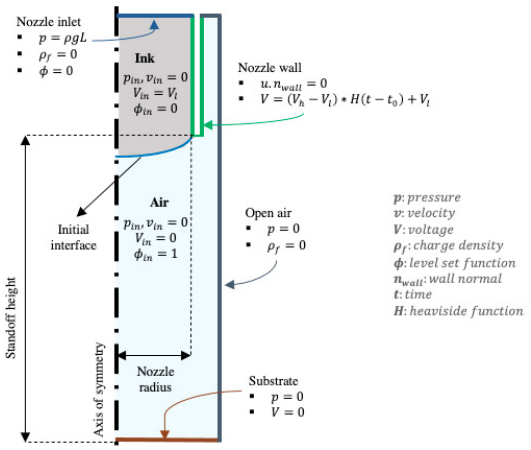

Fig. 3. **Model setup in COMSOL Multiphysics including the boundary conditions and the initial values.** Due to the axial symmetric assumption, the solver mirrors the solution around the axis of symmetry. Subscript "in" denotes the initial value, "l" and "h" denotes low and high, respectively.

occurs due to the interactions between two immiscible fluids and solid walls of a thin tube, where the resulting force can either oppose or contribute to the fluid travel along the tube depending on the interactions of the two fluids on the solid material, as explained in the previous section. This driving or opposing force in COMSOL can be introduced as the "wetted wall" boundary condition, which enforces the no-penetration condition, i.e. $u.n_{wall} = 0$ and adds a force to the wall (F_{wall} defined in eq. (12)). A suitable choice for β in this equation is the mesh element size.

The initial condition for the simulation starts the ink at equilibrium within the nozzle. This includes a low applied voltage and a spherical cap interface shape.

Once the physics, boundary conditions and initial values have been incorporated into the model, a mesh must be determined. It should be noted that there is always a trade-off between the precise dynamics captured by the model and simulation time.

4. SIMULATION RESULTS AND DISCUSSION

This section presents the simulation results for a high-resolution e-jet setup shown in Fig. 1. A sensitivity analysis for some of the key material parameters is also presented. The simulation model includes a 30 μm nozzle diameter with a 5 cm length (L), and a 150 μm standoff height (distance between the nozzle and the substrate). The ink material used for the simulation is water and its material properties are provided in Table I.

Table 1. Material Properties of Water

Material Property	Symbol	Value	Unit
Density	ρ	997	kg/m^3
Viscosity	μ	1	$mPa.s$
Relative permittivity	ε	80	1
Surface tension	γ	0.072	N/m
Contact angle on glass	θ	≈ 0	$degree$

The low and high voltages applied to the nozzle wall are 630 V and 1400 V, respectively, with the high voltage

applied at $t_0 = 1\ \mu s$. A regular nozzle length is roughly 5 cm leading to a boundary condition at the nozzle inlet of a hydrostatic pressure, $p = 490\ Pa$. The maximum mesh size used is 1.8 μm and the minimum mesh size is 3.6 nm. The simulation is conducted with a step size of 1 μs. Depending on the setup and material properties, the mesh size and the step size may need to be refined. For instance, for ink materials with higher viscosity, such as glycerol, we might be able to use coarser mesh and step size since the jetting dynamics occur slowly due to the high resistance to transitioning into a jetting state.

4.1 Simulation results:

The results of the simulation are presented in Fig. 4 and Fig. 5. Figure 4 shows that the ink material is at equilibrium at low voltage, meaning that the voltage is not enough to overcome the surface tension that is opposing the electric force. In fact, the pressures due to the surface tension and the viscosity are high enough to cancel the opposing pressures, including the hydrostatic pressure, the electric pressure and the capillary pressure. However, when a high voltage signal is applied, the electric force at the interface becomes stronger and deforms the meniscus shape from a spherical cap shape in equilibrium to a conical shape (Taylor Cone). Moreover, since the pulse width of the high voltage signal is long enough for the ink material to keep accumulating charge at the ink-air interface, the electric field can evolve the meniscus until the electric force overcomes the surface tension of the material and creates a jet toward the grounded substrate (t=80 μs in Fig. 4).

Figure 5 shows plots of volume fraction, electric potential, velocity and charge density at time=80 μs, for the same setup. In the velocity plot, it can be seen that the jet has a relatively high velocity ($\approx 3m/s$) along the jet close to the nozzle tip, and increases as the jet nears the substrate($\approx 4m/s$). At the nozzle inlet, a relatively low velocity ($\approx 0.2\ m/s$) transports the ink material inside the nozzle. Moreover, the charge density plot shows that the electric charge accumulates at the ink-air interface, close to the Taylor Cone, where the electric field is stronger than other regions.

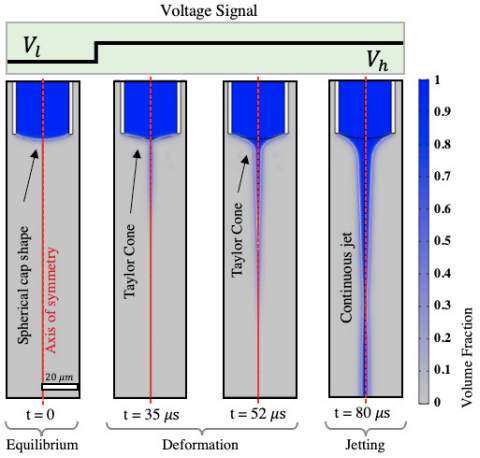

Fig. 4. The ink volume fraction plot of the simulated e-jet process for a 30 μm nozzle size with a 150 μm standoff height for different phases of jetting.

4.2 Sensitivity of key material parameters

To evaluate the impact of key parameters on model outcome, we conducted a sensitivity analysis on viscosity, surface tension, and relative permittivity. For the first study, all material properties and model setup conditions were held constant, while we varied the viscosity (see Fig. 6i). This study provides an understanding of key material parameters on the e-jet printing process separately. Figure 6i shows the volume fraction plot at time= 54 μs for varying viscosity. As can be seen in this figure, a higher viscosity results in a higher resistance of the ink material to jetting that can contribute to a slower jet for a high viscous material. In fact, by increasing the viscosity, the viscous force term in the Navier-Stokes equation increases in the opposing direction of jetting. In this situation, the electric force needs to get stronger to overcome the viscosity force (see Fig. 6i (c)), which could be either a stronger electric potential to apply or a longer pulse width to let more charge accumulate at the ink-air interface.

For the second study, we used a similar setup and material parameters as those mentioned in section IV, while varying the surface tension coefficient, γ. The simulation results at time= 53 μs are presented in Fig. 6ii. The second study considers three different surface tensions, including 0.05, 0.072 and 0.09 N/m. It is shown that a lower surface tension leads to an earlier jet with a thicker Taylor cone, while a high surface tension creates a slower jet and a thinner Taylor cone. This is because the ink material with a lower surface tension is dominated by the electric force during the e-jet process, which leads to the accumulated charge at the ink-air interface to be more effective resulting in more material jetting toward the substrate.

For the last study, the only varying parameter is relative permittivity of the ink material. Figure 6iii demonstrates the process at time= 67 μs. The simulation is conducted for relative permittivities of 60, 80, and 100 to show the impact of relative permittivity on the jetting process. It is demonstrated that as the relative permittivity increases, the jetting occurs faster. In fact, a higher relative permittivity results in a stronger electric force that accumulates sufficient charge at the meniscus in a shorter time at which they reach the same jetting volume.

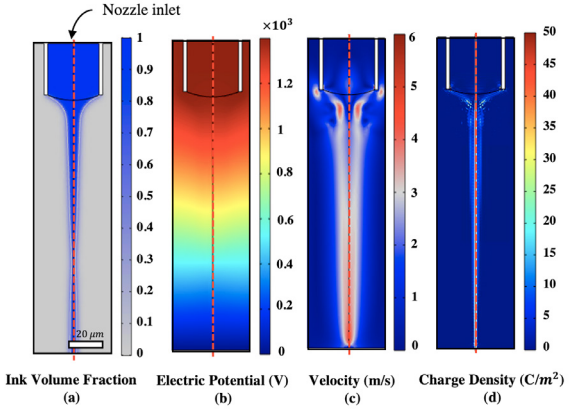

Fig. 5. **t = 80 μs. Simulation results of e-jet dynamics under a pulse voltage signal for water using a 30 μm nozzle** (a) ink volume fraction, (b) electric potential, (c) velocity, and (d) charge density.

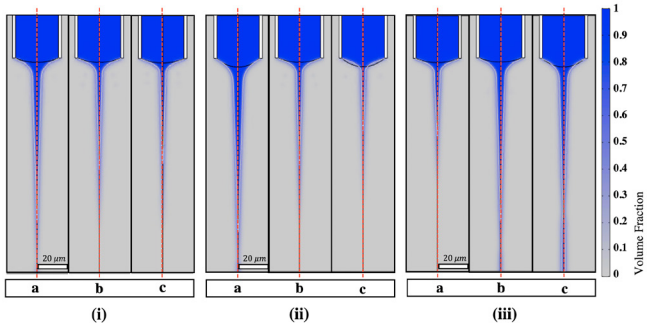

Fig. 6. **Ink volume fraction simulation results for the sensitivity study of the key material parameters. (i) Effect of viscosity**, time= 54 μs for the same setup while varying viscosity: (a) 0.8, (b) 1, and (c) 1.2 $mPa.s$. Increasing viscosity increases the ink material's resistance to deforming. **(ii) Effect of surface tension**, time= 53 μs for the same setup while varying surface tension: (a) 0.05, (b) 0.072, and (c) 0.09 N/m. Increasing surface tension results in a slower jet.**(iii) Effect of relative permittivity**, time= 67 μs for the same setup while varying while varying relative permittivity: (a) 60, (b) 80, and (c) 100. Increasing relative permittivity results in an earlier jet.

5. CONCLUSIONS

A high-fidelity framework is presented for modeling a high-resolution e-jet process using the leaky-dielectric model to describe the physics and the level set method to track the two-phase interface. The simulation results are in good agreement with the physics logic and the experimental observations of the process. The presented framework is capable of predicting the e-jet process behavior for any combinations of material and setup providing a platform for optimizing the tuning of e-jet parameters to get the desired jetting behavior. Moreover, this framework can be used to evaluate a simplified model for control design of the e-jet process. It should be taken into account that the current model can only predict the jetting dynamics, while the e-jet printing process is the result of droplet ejection, droplet spread and its coalescence behavior. Therefore, integrating this model with another model that is capable of capturing the material spread on the substrate could be an insightful next step. In the future, potential applications for this model range from microfluidics to control design, where it can be used to create simplified or machine-learning based models for e-jet or evaluate other models, such as control-oriented data-driven models.

REFERENCES

Cho, T.H., Farjam, N., Allemang, C.R., Pannier, C.P., Kazyak, E., Huber, C., Rose, M., Trejo, O., Peterson, R.L., Barton, K., and Dasgupta, N.P. (2020). Area-selective atomic layer deposition patterned by electrohydrodynamic jet printing for additive manufacturing of functional materials and devices. *ACS Nano*, 14, 17262–17272.

Farjam, N., Cho, T.H., Dasgupta, N.P., and Barton, K. (2020). Subtractive patterning: High-resolution electrohydrodynamic jet printing with solvents. *Applied Physics Letters*, 117, 133702.

Lastow, O. and Balachandranb, W. (2006). Numerical simulation of electrohydrodynamic (EHD) atomization. *Journal of Electrostatics*, 64, 850 – 859.

Melcher, J.R. and Taylor, G.I. (1969). Electrohydrodynamics: A review of the role of interfacial shear stresses. *Annual Review of Fluid Mechanics*, 1, 111–146.

Mohammadi, K., Movahhedy, M.R., and Khodaygan, S. (2019). A multiphysics model for analysis of droplet formation in electrohydrodynamic 3d printing process. *Journal of Aerosol Science*, 135, 72–85.

Onses, M.S., Sutanto, E., Ferreira, P.M., Alleyne, A.G., and Rogers, J.A. (2015). Mechanisms, capabilities, and applications of high-resolution electrohydrodynamic jet printing. *Small*, 11, 4237–4266.

Pan, Y. and Zeng, L. (2019). Simulation and validation of droplet generation process for revealing three design constraints in electrohydrodynamic jet printing. *Micromachines*, 10.

Pannier, C.P., Diagne, M., Spiegel, I.A., Hoelzle, D.J., and Barton, K. (2017). A dynamical model of drop spreading in electrohydrodynamic jet printing. *Journal of Manufacturing Science and Engineering*, 139, 111008.

Pannier, C.P., Wu, M., Hoelzle, D., and Barton, K. (2019). A dynamical model of drop spreading in electrohydrodynamic jet printing. *2019 American Control Conference (ACC)*.

Park, J., Hardy, M., Kang, S.J., Barton, K., Adair, K., k. Mukhopadhyay, D., Lee, C.Y., Strano, M., Alleyne, A.G., Georgiadis, J.G., Ferreira, P.M., and Rogers, J.A. (2007). High-resolution electrohydrodynamic jet printing. *Nature Materials*, 6, 782–789.

Roghair, I., Musterd, M., van den Ende, D., Kleijn, C., Kreutzer, M., and Mugele, F. (2015). A numerical technique to simulate display pixels based on electrowetting. *Microfluid Nanofluid*, 19, 465 – 482.

Saville, D.A. (1997). Electrohydrodynamics: The taylor-melcher leaky dielectric model. *Annual Review of Fluid Mechanics*, 29, 27–64.

Singh, S.K. and Subramanian, A. (2020). Phase-field simulations of electrohydrodynamic jetting for printing nano-to-microscopic constructs. *RSC Advances*, 10, 25022.

Spiegel, I.A., Kovalenko, I., Hoelzle, D., Sammons, P.M., and Barton, K.L. (2017). Hybrid modeling and identification of jetting dynamics in electrohydrodynamic jet printing. *2017 IEEE Conference on Control Technology and Applications (CCTA)*.

Spiegel, I.A., Sammons, P., and Barton, K. (2020). Hybrid modeling of electrohydrodynamic jet printing. *IEEE Transactions on Control Systems Technology*, 28, 2322–2335.

Wright, G.S., Krein, P.T., and Chato, J.C. (1993). Factors affecting dynamic electrical manipulation of menisci. *IEEE Trans. Ind. Appl.*, 29, 103–112.

Yang, J., Kim, H., Cho, B., and Chung, J. (2014). Modeling of sessile droplet oscillation on electrohydrodynamic jetting nozzle at constant back pressure. *J. Mech. Sci. Technol.*, 28, 2815–2823.

Zhao, X., Wang, D., Lin, Y., Y.Sun, T.Ren, Liang, J., and Madou, M. (2019). Numerical simulation of coaxial electrohydrodynamic jet and printing nanoscale structures. *Microsystem Technologies*, 25, 4651–4661.